Case Studies in Construction Materials 24 (2026) e05875

Contents lists available at ScienceDirect

Case Studies in Construction Materials

journal homepage: www.elsevier.com/locate/cscm

Carbonation curing of ultra-high-performance concrete produced with Portland cement of varying belite content

Joonho Seo [a], G.M. Kim [b], Jihoon Park [a], Jin-Ho Bae [a,c,d], Naru Kim [a], Sungsik Choi [a], H.K. Lee [a,*]

[a] Department of Civil and Environmental Engineering, Korea Advanced Institute of Science and Technology (KAIST), 291 Daehak-ro, Yuseong-gu, Daejeon 34141, Republic of Korea
[b] Mineral Processing & Metallurgy Research Center, Resources Utilization Division, Korea Institute of Geoscience and Mineral Resources, 124 Gwahak-ro, Yuesong-gu, Daejeon 34132, Republic of Korea
[c] Department of Mechanical Engineering, Ulsan National Institute of Science and Technology, Ulsan 44919, South Korea
[d] KAIST InnoCORE PRISM-AI Center, Korea Advanced Institute of Science and Technology, 291 Daehak-ro, Yuseong-gu, Daejeon 34141, South Korea

ARTICLE INFO

Keywords:
Ultra-high-performance concrete
Carbonation curing
Portland cement types
Microstructure
Mechanical properties

ABSTRACT

This study explores the potential application of carbonation curing to ultra-high-performance concrete (UHPC) produced with Portland cement of varying belite content. After an initial curing phase, the UHPC samples underwent either steam curing at 90 °C or carbonation curing under a 5 % CO_2 concentration. Test results indicated that the mechanical strength of the carbonation-cured UHPC samples was generally lower than that of the steam-cured counterparts. Among all cement types, the UHPC samples made with type III cement exhibited the highest strength regardless of the curing regime and/or age. Carbonation curing significantly altered both clinkers and hydrates, with the most pronounced changes observed in the UHPC samples made with type IV cement, suggesting high levels of CO_2 ingress and uptake. In addition, as silica fume contributed minimally to the reactions in the carbonation-cured UHPC samples, microstructural development was primarily driven by the carbonation of clinkers, which led to the formation of C-S-H and Ca-modified SiO_2 and the precipitation of $CaCO_3$. While steam curing was found to accelerate the reaction of clinkers in a limited timeframe, type IV cement demonstrated potential advantages as part of a carbonation curing strategy when considering environmental benefits. These results suggest that the carbonation curing of UHPC, particularly with belite-rich cement, could provide a low-energy and low-carbon alternative to conventional steam curing practices, thereby offering practical value for sustainable construction applications.

1. Introduction

Ultra-high-performance concrete (UHPC) is a well-known advanced cementitious material that exhibits superior mechanical and durability properties, making this material a highly sought-after component in modern construction [1–3]. UHPC can be characterized by its ultra-high compressive strength, often exceeding 120 MPa; exceptional tensile strength (mainly due to fiber reinforcement); and its outstanding durability performance against harsh conditions [4,5]. These properties are achieved through the formation of a dense

* Corresponding author.
E-mail address: haengki@kaist.ac.kr (H.K. Lee).

https://doi.org/10.1016/j.cscm.2026.e05875
Received 31 July 2025; Received in revised form 11 September 2025; Accepted 6 February 2026
Available online 7 February 2026

microstructure, optimized particle packing, low water-to-binder ratios, and the proper incorporation of supplementary cementitious materials [5–8]. Due to these characteristics, UHPC is widely utilized in infrastructure projects demanding extended service times, such as long-span bridges, high-rise buildings, marine structures, and defense applications where resilience under extreme conditions is essential [9–11].

Despite its remarkable advantages, the production of UHPC presents significant challenges, particularly regarding the curing processes [12,13]. Steam curing is conventionally employed to accelerate hydration and promote rapid strength development at early ages [13,14]. However, steam curing strategies generally require substantial energy input to maintain and secure high temperatures and humidity levels, leading to increased production costs and a considerable carbon footprint [12,13]. The reliance on steam curing not only exacerbates environmental concerns by contributing to CO_2 emissions but also possibly limits the broader applications of UHPC in the future due to economic constraints. Consequently, identifying alternative and sustainable curing methods is critical to enhancing the viability of UHPC in modern construction.

Carbonation curing has emerged as a promising technique, offering both environmental and performance benefits [15–18]. This method involves exposing fresh/hardened cementitious materials to concentrated CO_2, which reacts with calcium-bearing components to form calcium carbonates, improving the durability and strength development at early ages while simultaneously sequestering CO_2 [15–18]. Beyond enhancing the strength, carbonation curing can refine the microstructure by reducing the degree of porosity, thereby strengthening the long-term durability and contributing to sustainability efforts by realizing the safe and efficient geological storage of CO_2 into cementitious materials [19,20]. Given these advantages, carbonation curing is gaining traction as a viable approach to improving both the ecological footprint and performance of cementitious materials [21,22].

To mitigate the environmental impact of using conventional steam curing during the manufacturing of UHPC, researchers have explored alternative curing techniques especially for UHPC [23]. These include ambient curing supplemented with chemical activators [23], autoclave curing for rapid strength development [24,25], and internal curing strategies utilizing pre-saturated lightweight aggregates [26,27] or superabsorbent polymers [28,29]. Beyond the modification of curing regimes, several recent studies [30–32] have sought to incorporate geopolymeric binders into UHPC systems, thereby offering a pathway toward sustainable production with a markedly lower carbon footprint, without compromising engineering aspects. The aim of each method is to optimize the performance of UHPC while reducing the amount of energy consumed. However, challenges related to scalability, efficiency, and cost-effectiveness remain, necessitating further research into viable solutions. Integrating carbonation curing into UHPC production represents an innovative and novel research direction [33–35]. Unlike conventional methods, carbonation curing has the potential to enhance strength development at early ages while significantly reducing energy demands and greenhouse gas emissions [36]. Investigating the feasibility of carbonation curing for UHPC presents several scientific challenges, including understanding its effects on mechanical performance outcomes and microstructural evolution [33–35]. The introduction of carbonation curing as an alternative curing method to UHPC production stands out by bridging the gap between sustainability and high-performance concrete technology, leveraging carbonation curing to optimize the production processes of UHPC.

Cements with a high alite content are known for their rapid strength development and high hydration reactivity; however, they are also associated with long-term durability concerns [37–40]. In contrast, belite-rich cements offer environmental benefits, such as lower optimal clinkerization temperatures and reduced CO_2 emissions, but their lower reactivity limits early strength development [41–43]. Therefore, when developing new materials, it is essential to evaluate the feasibility of using cements with varying alite and belite contents. In particular, there are rationales for investigating the hydration and carbonation characteristics of different types of cement. By incorporating cements with different belite contents, this study aims to systematically analyze how belite influences the physicochemical properties of UHPC, particularly in relation to carbonation curing. Several works have investigated the interaction of belite with carbonation curing. Jang and Lee [44] demonstrated that the carbonation curing of belite-rich cements can lead to extensive precipitation of $CaCO_3$ and remarkable microstructural densification, resulting in the compressive strength enhancement of 172 %.

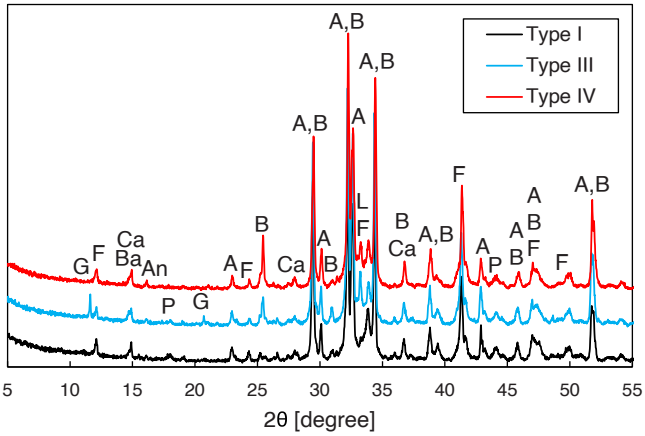

Fig. 1. XRD patterns of the raw Portland cement samples: G- gypsum, F- brownmillerite, Ca- calcite, Ba- basanite, An- anhydrite, P- periclase, A- alite, B- belite, and L- lime.

Guan et al. [45] further showed strength increase by up to 80 % through the carbonation curing of belite-rich cement. Consistently, Kim et al. [46] revealed that belite-rich cement exhibits faster CO2 uptake and superior strength gain than type I PC under carbonation curing, confirming its suitability for low-carbon and high-performance concrete production.

Given that previous research suggests carbonation may enhance the hydration reactivity of belite [47,48], this study seeks to explore the potential of carbonation as a means to improve the performance and applicability of belite-rich cement in ultra-high-strength concrete.

The present study aims to evaluate the influence of carbonation curing on the properties of UHPC by examining the effects of various types of Portland cement on the microstructure, strength development, and carbonation behavior of these materials. By addressing the knowledge gap in the carbonation curing of UHPC, this research contributes to advancing sustainable construction materials and provides valuable insights into achieving an optimal balance between mechanical performance and environmental responsibility.

2. Experimental program

2.1. Raw materials and sample fabrication

Three different types of Portland cement (types I, III, and IV [49]) were used in this study. All types of Portland cement utilized in this study were supplied by SsangYong Cement Industrial Co., Ltd., and their X-ray diffractometry (XRD) patterns are presented in Fig. 1. Additionally, X-ray fluorescence and Rietveld quantitative XRD analysis results of the Portland cement samples are summarized in Table 1. It was observed that the type III and type IV cements have significantly higher alite and belite contents, respectively, compared to the type I cement.

Three types of Portland cement, silica fume, silica powder, and silica sand were used as powders in the UHPC mixtures. The SiO_2 contents of the silica fume and silica powder were 96.8 % and 94.3 %, respectively. In the UHPC matrix, silica fume contributes to strength development by participating in pozzolanic reactions with PC to form additional C-(A)-S-H [50], whereas the silica powder was used as a filler of UHPC, which can enhance packing density and strength development. The particle size distributions of the silica fume, silica powder, and silica sand are shown in Fig. 2. The mixture proportions of the UHPC samples are presented in Table 2. Silica fume and silica powder were incorporated at 25 % by weight of the Portland cement. A high-range water reducer superplasticizer specifically designed for UHPC, manufactured by Dongnam Chemical Company, was used in this study in order to secure proper workability. The UHPC mixture design served to achieve high workability with a target slump flow rate exceeding 750 mm, ensuring smooth casting and application. Paste samples for chemical analyses were also prepared, with all conditions identical except for the exclusion of silica sand. The use of steel fibers, which are commonly included in UHPC, was omitted in this study to simplify the sample preparation, as the focus was primarily on hydration characteristics. The UHPC samples were used for compressive and flexural strength measurements and for a carbonation depth evaluation, while the paste samples were utilized for XRD, thermogravimetry (TGA), and ^{29}Si magic-angle spinning (MAS) nuclear magnetic resonance (NMR) analyses.

Sample casting was performed as follows. Firstly, Portland cement, silica fume, and silica powder were mixed for approximately 5 min. Simultaneously, a solution of water and superplasticizer was prepared. The dry-mixed powder mixture and the combined solution were then agitated for an additional 10 min to ensure the integration of the superplasticizer. Afterward, silica sand was added and the mixture was agitated for further 10 min. It should be noted that the paste samples were fabricated without the addition of silica sand. The UHPC samples for the compressive and flexural strength tests were cast into $50 \times 50 \times 50$ mm^3 cube molds and $40 \times 40 \times 160$ mm^3 prism molds, respectively. The fresh-state UHPC samples were manually compacted using a rubber rod. The carbonation depth evaluation was performed using $40 \times 40 \times 160$ mm^3 prisms. Paste samples for the chemical analyses were cast into $25 \times 25 \times 25$ mm^3 cube molds.

Table 1
Chemical and mineral compositions (wt%) of the Portland cements used in this study.

Chemical composition				Mineral composition			
	Cement type				Cement type		
	Type I	Type III	Type IV		Type I	Type III	Type IV
CaO	62.5	62.1	62.5	C_3S	51.2	56.3	40.6
SiO_2	21.0	19.7	25.3	C_2S	18.8	12.6	34.6
Al_2O_3	5.9	5.9	3.1	C_3A	3.1	3.4	3.3
Fe_2O_3	3.2	3.0	3.6	C_4AF	11.2	11	11.8
SO_3	2.1	4.2	2.0	Calcite	7.6	4.9	1.2
R_2O	0.8	0.6	0.5	Portlandite	1.4	4.0	-
				Periclase	3.0	2.4	3.2
				Basanite	2.7	2.4	3.6
				Anhydrite	0.3	0.9	1.5
				Gypsum	0.2	0.8	-
				Quartz	0.5	1.3	0.2

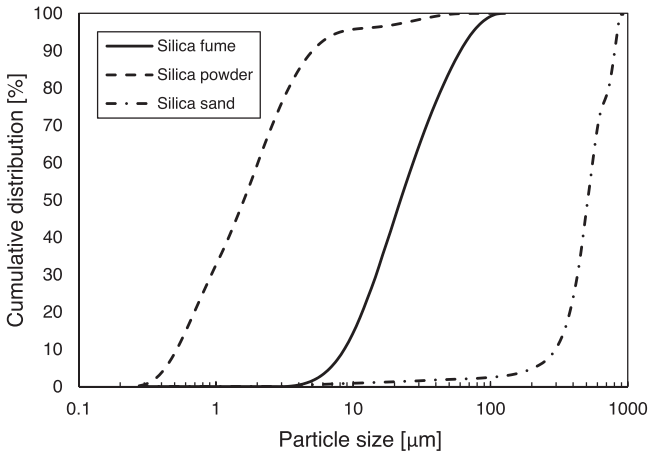

Fig. 2. Particle size distribution of the silica fume, silica powder, and silica sand used in this study.

Table 2
Mixture proportion of the UHPC samples used in this study (wt%).

Portland cement (Type I, III, or IV)	Silica fume	Silica powder	Silica sand	Water	Superplasticizer
100	25	25	110	21	4

2.2. Curing condition and sample treatment

After casting, the samples were wrapped entirely with plastic bags and subjected to initial curing for 1 d (25 °C). Following this initial curing period, the samples were divided into two groups: one subjected to steam curing and the other to carbonation curing. The steam-cured samples were placed in a steam curing chamber for 2 d after the initial curing period. The environment of the steam curing chamber was maintained at an average temperature of 90 °C and 100 % relative humidity. After 2 d of steam curing, the samples were removed from the steam curing chamber, sealed with plastic bags, and stored in a temperature-controlled chamber at 25 °C for the subsequent curing period. On the other hand, the carbonation-cured samples were transferred after initial curing to an accelerated carbonation chamber maintained at a 5 % CO_2 concentration, a temperature of 25 °C, and 70 % relative humidity. It should be noted that temperature was controlled via refrigeration cycle and electric heater, and humidity was regulated by automatically spraying water vapor into air stream inside the chamber. In addition, CO_2 concentration monitoring sensors attached in the middle of the chamber controlled the CO_2 gas inlet flow to maintain the target CO_2 concentration. The carbonation-cured samples were carbonated for additional 27 d. To guarantee the uniform carbonation on all surfaces of the samples, the samples were elevated approximately 10 mm from the chamber floor using thin metal rods during carbonation. Paste samples for the chemical analyses were manually ground to reach a maximum particle size of less than 10 mm before being placed in the steam or carbonation curing chamber. At the designated curing ages for the chemical analyses, the paste samples were ground further using a mortar and pestle and sieved through a 73 μm mesh. The resulting powder was then treated with isopropanol and diethyl ether to halt hydration [51].

2.3. Characterization methods

The mechanical strength of UHPC samples was evaluated through compressive and flexural strength tests. The compressive strength was measured in accordance with the procedure specified in ASTM C109 [52] using a 100-ton compression machine. The loading rate was maintained at a constant 0.4 MPa/sec during the measurement. The flexural strength was assessed using a three-point bending test, as specified in ASTM C348 [53]. For both the compressive and flexural strength tests, the reported values represent the average of three measurements. These tests were conducted at 3, 7, 14, and 28 d of curing. It is worth noting that the strength measurements determined by ASTM C109 and C348 shall be interpreted as intrinsic material properties rather than directly compared with large-scale testing values as specified in ASTM C1856 [54].

The XRD analysis was conducted using an Empyrean diffractometer from Malvern Panalytical. The measurements used Cukα radiation with a step size of 0.0026° 2θ and a counting time of 1.56 sec per step. Quantification of the XRD patterns of the samples was done with Rietveld calculations (internal standard material method). The rutile (purity level > 99 %) was additionally incorporated into the samples for XRD at 10 wt%. The TGA analysis was carried out using a Q600 SDT analyzer from TA Instruments. Approximately 20 mg of each sample was placed in a crucible connected to a microbalance. The samples were heated from ambient temperature to 800 °C at a constant heating rate of 10 °C/min. Data were recorded for the percentage weight loss relative to the initial sample weight and the derivative of the weight loss percentage with respect to the temperature (%/°C). To assess the carbonation degree of the UHPC samples, a 1 % phenolphthalein solution was sprayed onto the cross-sections of perpendicularly split prismatic samples. The

carbonation of UHPC samples induces a pH reduction, leading to colorimetric differentiation between the carbonated and non-carbonated regions on the sprayed surface, as shown in Fig. 3(a). The resulting color change was captured and processed into binary colors using MATLAB software (Fig. 3(b)). Each region was segmented into pixels, and the carbonated and non-carbonated areas were quantified by counting the number of white and black pixels, respectively. The total cross-sectional area of the sample was determined by the total number of pixels, excluding the external background area, which was identified as black region in Fig. 3(c). The carbonation degree was then determined as the ratio of the carbonated area (number of white pixels in Fig. 3(b)) to the effective total cross-sectional area. This quantitative method, based on color differentiation, enables a comparison of carbonation ingress in the UHPC samples with different binder types and curing duration. The ^{29}Si MAS NMR spectra of the samples were acquired using a vertical-bore Bruker Avance III 400 MHz spectrometer. The measurements were performed at a Larmor frequency of 79.5 MHz with a spinning rate of 11 KHz. A 20-sec relaxation delay was applied between scans to allow for magnetization recovery. Tetramethylsilane was used as the reference standard for calibrating the chemical shift. A quantitative evaluation of the ^{29}Si NMR data was carried out through deconvolution, which was applied to each spectrum using Origin software. Initially, the ^{29}Si MAS NMR spectra of the three types of raw Portland cement, silica fume, and silica powder were deconvoluted. The spectra of the raw Portland cements were deconvoluted into five to seven individual peaks using a Gaussian function, while the spectra of the silica fume and silica powder were deconvoluted using Gaussian-Lorentz cross and Lorentz functions, respectively, each fitted using a single peak. The deconvolution data of the raw materials served as a foundation for deconvoluting the paste samples. The parameters of the raw material peaks, including full width at half maximum (FWHM), shape, and function, were used as baseline inputs. Reaction products were assigned to new Q^n sites, with the FWHM restrained at 5 ppm to ensure accurate deconvolution. For Ca-modified SiO_2, formed as a result of carbonation curing, the FWHM was restrained at 10 ppm to improve the precision and reliability of the deconvolution process. The deconvolution calculations were iterated until the reduced chi-square tolerance reached 10^{-9}.

3. Test results and discussion

3.1. Compressive and flexural strength

The compressive strength of the UHPC samples is shown in Fig. 4. Notably, the compressive strength of the steam-cured samples showed minimal changes after 3 d of curing. This phenomenon can be attributed to the significant progress of hydration of cement clinkers within the 2 d of steam curing period. The samples made with type III cement exhibited the highest compressive strength among the steam-cured samples across all measurement periods. It is interesting to note that the samples made with type IV cement, which has the highest belite content, showed the second-highest compressive strength after the samples made with type III cement upon steam curing. This observation clearly indicated that steam curing can vastly enhance the reactivity of belite. On the other hand, the samples made with type I cement demonstrated the lowest compressive strength. This may be partially due to the higher calcite content in type I cement compared to other cement types, which could hinder the hydration of clinkers. Hartmann and Plank [55] reported that aging of PC can lead to carbonates surface coatings due to native calcite or pre-carbonation which impede water access to clinkers and retard/hinder strength development. The compressive strength outcomes of the steam-cured UHPC samples made with the type I, III, and IV cement at 28 d of curing were 142.1 MPa, 170.2 MPa, and 166 MPa, respectively. In contrast, the compressive strength development of the carbonation-cured UHPC samples exhibited a different trend, showing a gradual increase even after 3 d of curing. Meanwhile, except for the strength observed at 3 d of curing, the samples made with type III cement consistently showed the highest compressive strength, followed by those made with type IV cement. However, the compressive strength values of the carbonation-cured samples were generally lower than those of the steam-cured samples at all curing ages. The compressive strength values of the carbonation-cured UHPC samples made with the type I, III, and IV cement at 28 d of curing were 104.5 MPa, 146.7 MPa, and 119.2 MPa, respectively, which correspond to 73.6 %, 86.2 %, and 71.8 % of the compressive strength of the steam-cured samples at an identical age, respectively.

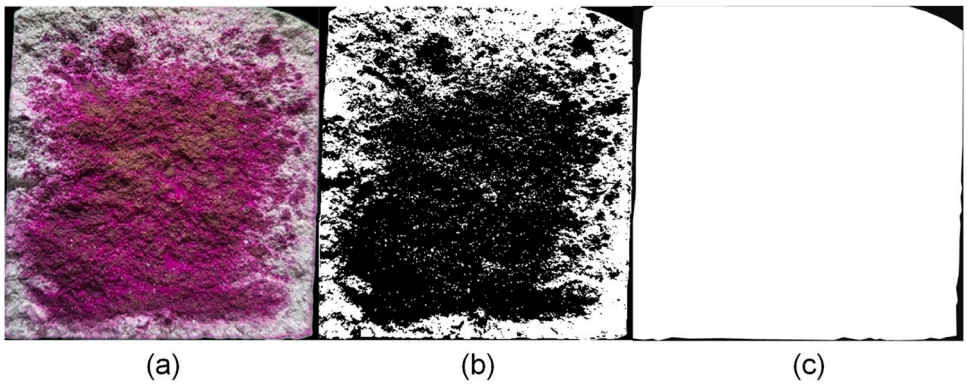

Fig. 3. Process for measuring the degree of carbonation of the UHPC samples: (a) colorimetric differentiation between carbonated and non-carbonated regions, (b) captured image processed into binary colors, and (c) exclusion of background area.

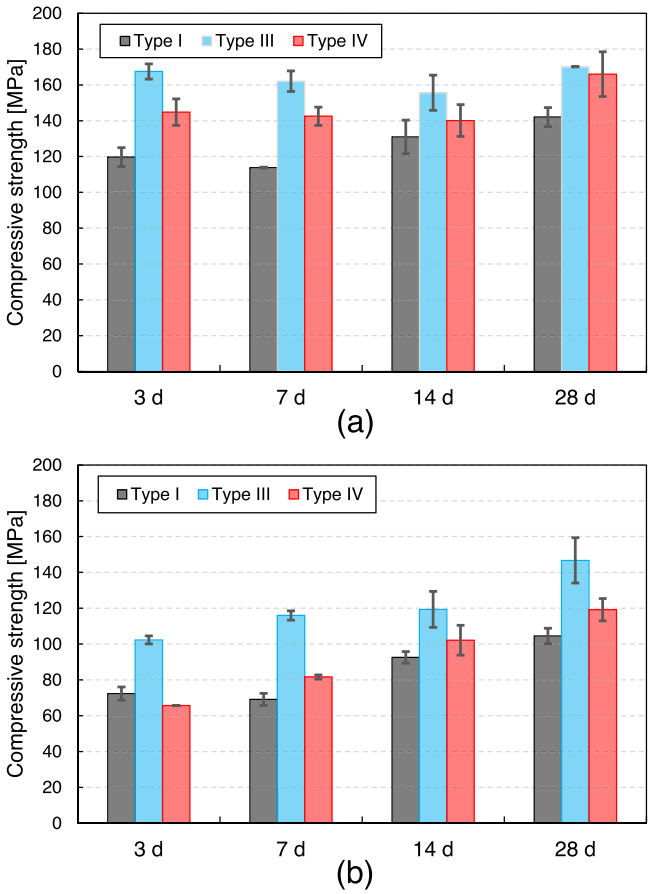

Fig. 4. Compressive strength development of the (a) steam-cured and (b) carbonation-cured UHPC samples. Error bars indicate the standard deviation from the mean of triplicate measurements.

The flexural strength of the UHPC samples is shown in Fig. 5. The flexural strength development of the steam-cured samples showed a continuous increase after 3 d of curing, which is different from the compressive strength development. However, the flexural strength of the steam-cured samples made with type III cement was highest at all measurements, identical to the trend found for the compressive strength development. On the other hand, the flexural strength of the steam-cured samples made with type IV cement was lowest at all ages. The stream-cured samples made with type I, III, and IV cement showed corresponding flexural strength outcomes of 19.4, 23.6, and 18.1 MPa at 28 d of curing. The flexural strength of the carbonation-cured samples showed a continuous increase with the curing age, similar to the trend observed when assessing the compressive strength development. No distinct pattern in the flexural strength development was observed until 14 d of curing. At 28 d of curing, the samples made with type III cement exhibited the highest flexural strength, followed by those made with type IV and I cement. The flexural strength of the carbonation-cured UHPC samples made with type I, III, and IV cement at 28 d of curing were 15.9 MPa, 20.0 MPa, and 18.1 MPa, respectively, which correspond to 81.8 %, 84.8 %, and 100 % of the flexural strength of the steam-cured samples at an identical age.

3.2. XRD

The XRD results of the UHPC paste samples are shown in Fig. 6. At 1 d of curing, all samples exhibited a hump-like feature corresponding to C-S-H at approximately 29.4° 2θ as the primary hydration product. No other hydration products were detected. Specifically, portlandite was absent, likely due to its consumption through a pozzolanic reaction with silica fume [56]. The peak intensity of C-S-H was significantly lower in the sample made with type IV cement, indicating that the degree of hydration remained low in the belite-rich cement at early curing stages. In addition to hydration products, peaks corresponding to unreacted cement clinkers, such as alite and belite, were observed in the patterns. Peaks assigned to quartz and calcite were also identified, likely originating from impurities or weathering of the raw cements.

The XRD results of the steam-cured samples at 7 d of curing revealed a significant reduction in the peak intensities corresponding to alite and belite, meaning a substantial increase in the reaction of clinkers. Despite this, the peak of belite remained more prominent than the peak of alite, and the peak intensity of C-S-H was highest in the sample made with type III cement. These findings suggest that type III cement exhibits the highest hydration degree under the steam curing regime. In contrast, the XRD results of the carbonation-

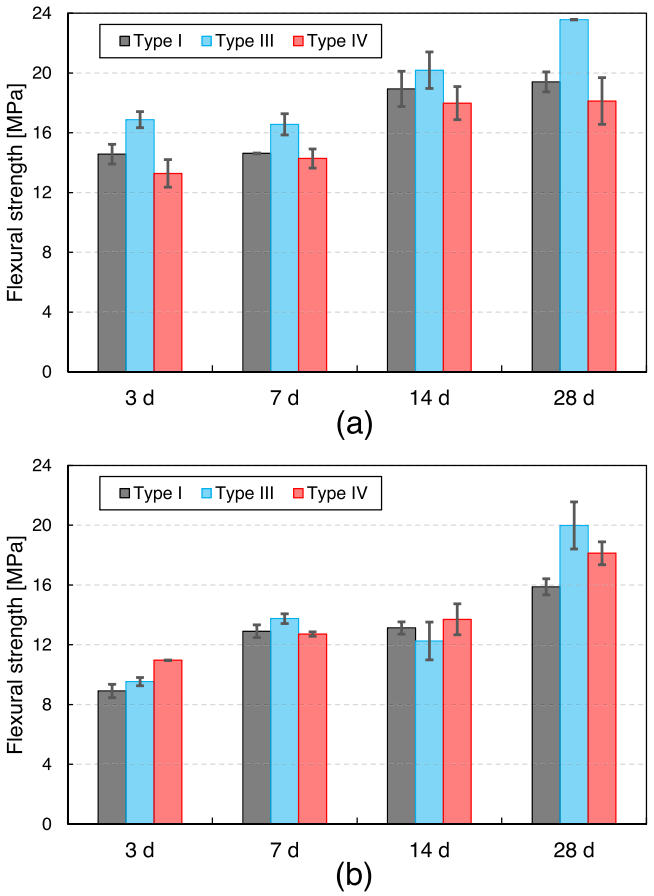

Fig. 5. Flexural strength development of the (a) steam-cured and (b) carbonation-cured UHPC samples. Error bars indicate the standard deviation from the mean of triplicate measurements.

cured samples at 7 d of curing displayed notable differences from those of the steam-cured samples. A distinct characteristic of the carbonation-cured samples was the pronounced peak intensity of calcite. Similar to the steam-cured samples, the peak intensities of alite and belite were significantly reduced compared to those of the samples at 1 d of curing, indicating that carbonation curing also contributed to enhancing the reactivity of clinkers. However, a key difference from the steam-cured samples was observed in the samples made with type I and IV cements, where the peak intensity of belite appeared greatly reduced. This suggests that carbonation curing may have influenced the reactivity of belite more compared to steam curing.

The XRD patterns of the samples at 28 d of curing exhibited no significant differences compared to those at 7 d of curing, regardless of the curing regime. However, in the steam-cured samples, the peak corresponding to C-S-H became sharper and more intense. These observations indicate that no new crystalline phases were formed with prolonged curing, whereas the existing phases continued to develop.

Phase quantification results of the samples through Rietveld calculations of the XRD patterns are presented in Fig. 7. The calcite content in the carbonation-cured samples increased gradually with the curing age across all samples, indicating that carbonation continued to progress over time. The increased amorphous content can be attributed to the growth of C-S-H in the steam-cured samples. In the carbonation-cured samples, however, it is likely that both decalcified C-S-H and Ca-modified SiO_2 were mainly reflected in the amorphous content [57], with some minor contents featured from the presence of silica fume. The amorphous content in both the steam- and carbonation-cured samples increased rapidly during the initial 7 d but exhibited a much slower rate of increase after 7 d of curing.

3.3. TGA

The TGA results of the UHPC paste samples are shown in Fig. 8. The weight losses of all samples were classified according to three major temperature ranges: around 100 °C, approximately 400 °C, and beyond 600 °C. The weight loss near 100 °C is primarily attributed to the dehydration of C-S-H and ettringite [58], as corroborated by the XRD results. Notably, the steam-cured samples exhibited more weight loss in this temperature range compared to the carbonation-cured samples, likely due to the decalcification of C-S-H induced by carbonation [59]. Among the carbonation-cured samples, the greatest changes in the DTG curve within this

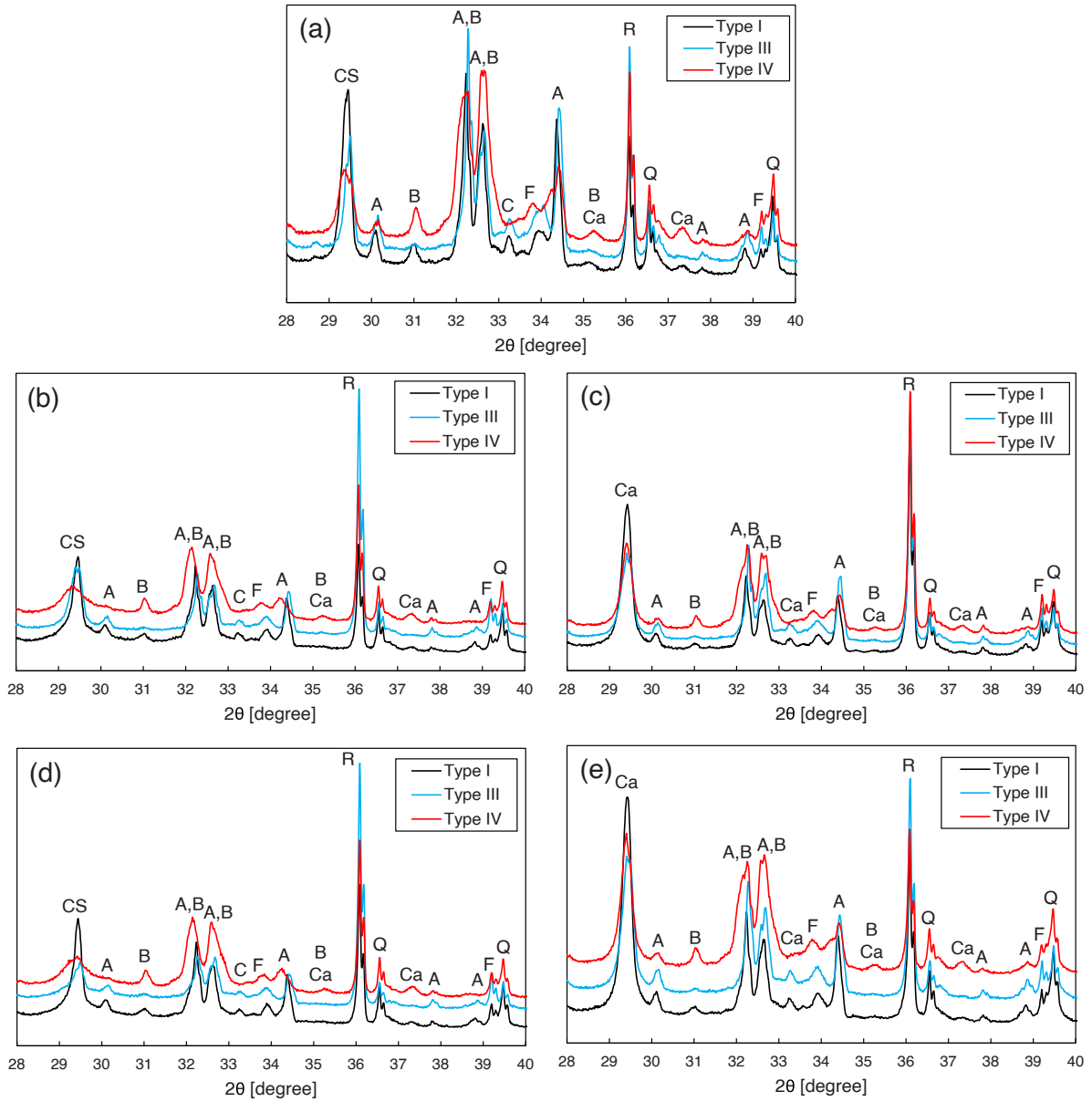

Fig. 6. X-ray diffractometry results of the UHPC paste samples at (a) 1 d of curing, (b) steam- and (c) carbonation-cured UHPC paste samples at 7 d of curing, and (d) steam- and (e) carbonation-cured UHPC paste samples at 28 d of curing. CS- calcium silicate hydrate, A- alite, B- belite, C- C_3A, F- C_4AF, Ca- calcite, R- rutile (internal standard), and Q- quartz.

temperature range compared to the steam-cured samples was observed in the samples made with type I cement, followed by the samples made with type IV cement, whereas the samples made with type III cement showed minimal variation. This suggests that the extent of carbonation was highest in the samples made with type I cement. The weight loss that occurred near 400 °C corresponds to the dehydroxylation of portlandite [60], which was distinctly observed only in the samples at 1 d of curing. At later ages, the presence of portlandite was no longer detectable, possibly due to its complete consumption through the pozzolanic reaction with silica fume in the steam-cured samples or its depletion due to carbonation in the carbonation-cured samples. The weight loss that occurred beyond 600 °C is attributable to the decarbonation of carbonates [61]. This weight loss was clear in the carbonation-cured samples, indicating the formation of carbonates (mainly calcium carbonate) due to the carbonation of hydration products or clinkers. The most substantial weight loss associated with the decarbonation of carbonates was observed in the samples made with type I cement, further confirming that the extent of carbonation was most severe in these samples. The enhanced mechanical properties of carbonation-cured Portland cement-based materials is generally known to stem from the packing effect induced by the precipitation of carbonates [62]. In this study, however, the samples made with type III cement, which exhibited the lowest extent of carbonation, demonstrated the highest

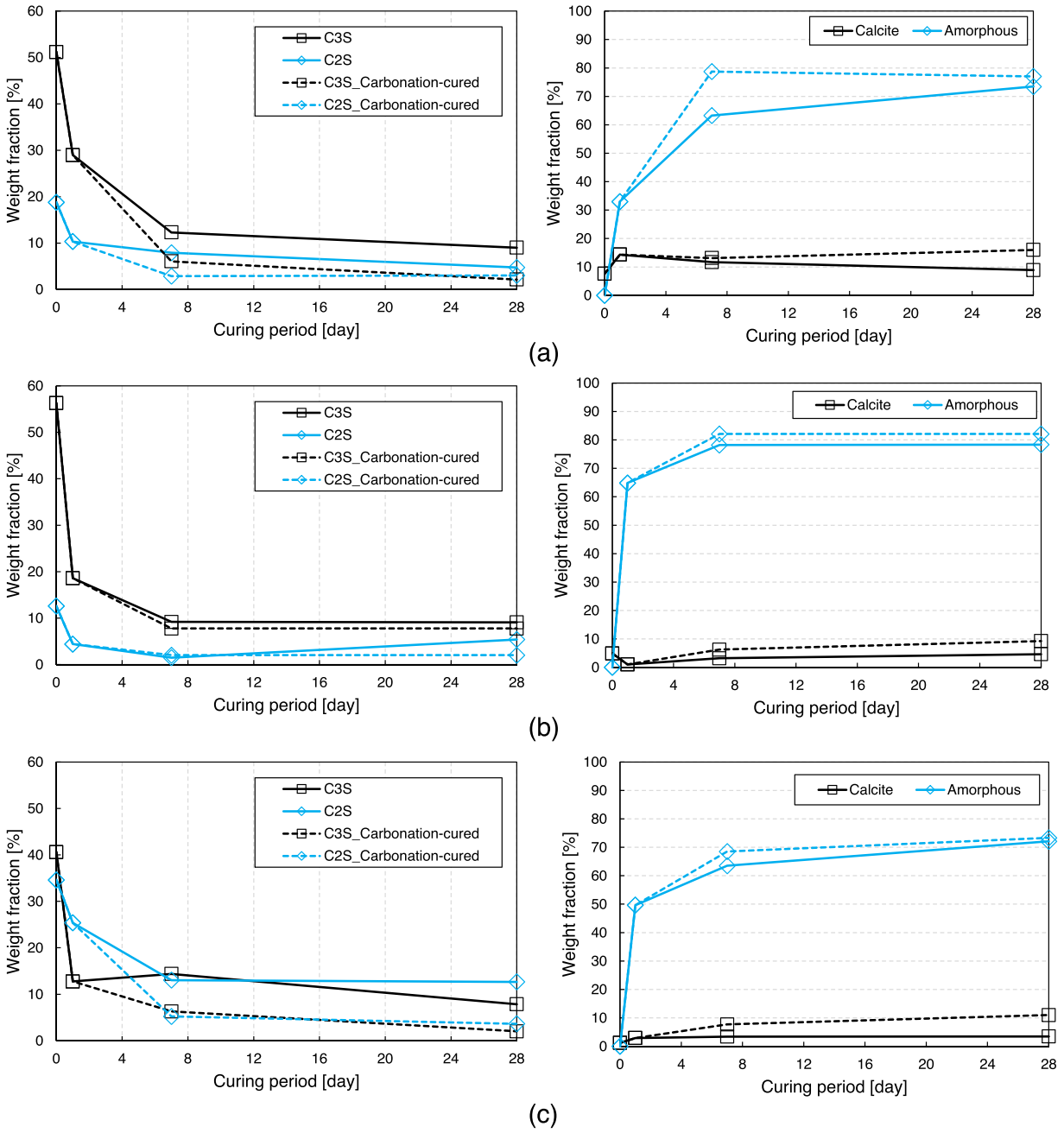

Fig. 7. Quantification of the C_3S, C_2S, calcite, and amorphous contents (wt%) in the UHPC paste samples made with type (a) I, (b) III, and (c) IV Portland cement as calculated by the Rietveld calculation of XRD patterns of the samples. Solid and dotted lines indicate the quantification results of the steam- and carbonation-cured samples, respectively.

compressive and flexural strength outcomes. This suggests that carbonation curing may not be an effective approach for the fabrication of UHPC when using type III cement given that UHPC made with type III cement is less influenced by carbonation curing. Instead, carbonation curing is likely to be more effective in terms of CO_2 uptake when applied to UHPC made with type I or IV cement rather than type III cement.

3.4. Carbonation depth

The cross-section carbonation degree of the carbonation-cured UHPC samples at 28d of curing is shown in Fig. 9. Through this test, the extent of CO_2 ingress toward the center of the carbonation-cured samples can be compared by analyzing pH variations [63,64]. It

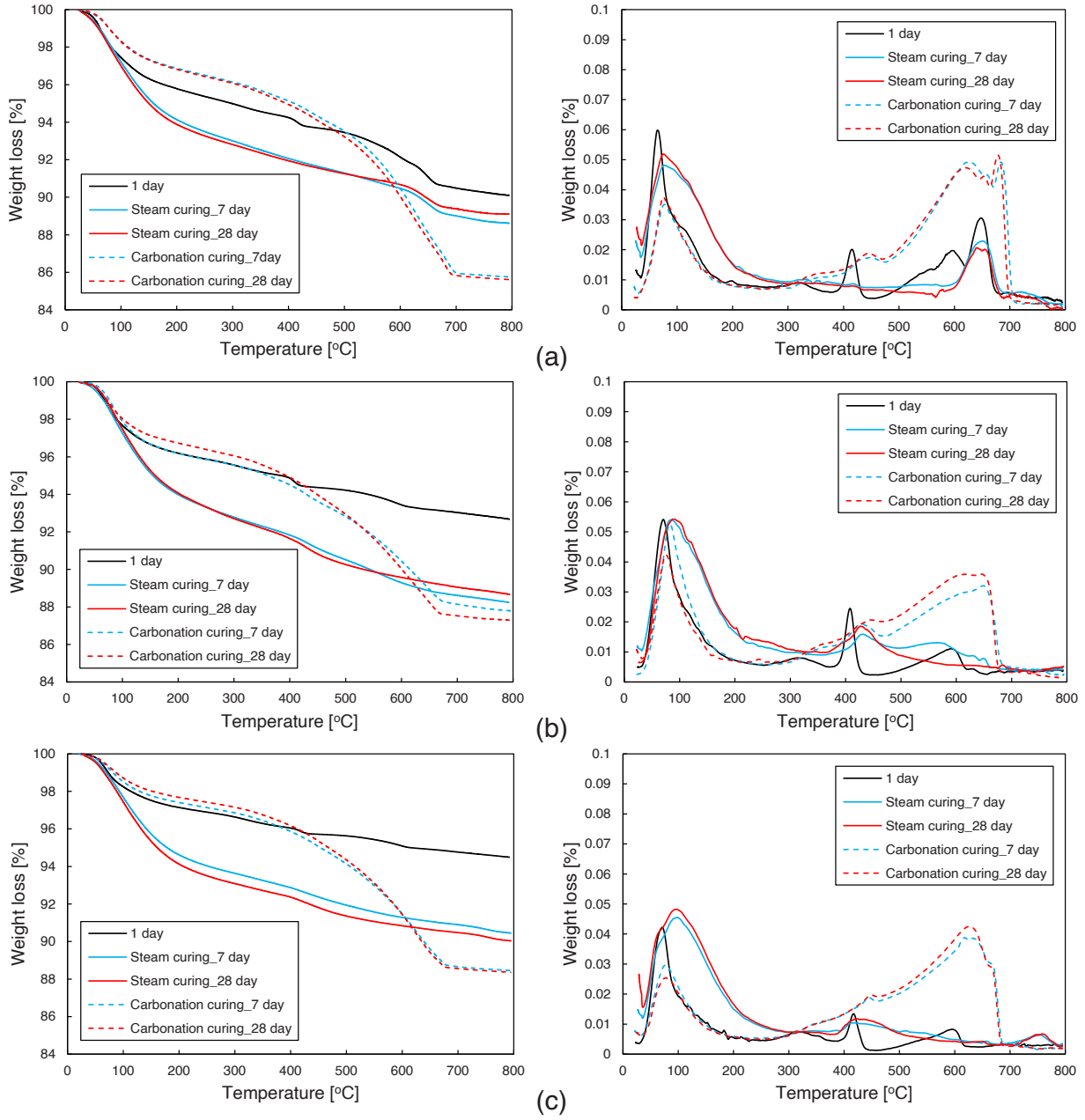

Fig. 8. Thermogravimetry analysis of the UHPC paste samples made with type (a) I, (b) III, and (c) IV Portland cement.

was clearly observed that the degree of carbonation was highest in the samples made with type I cement across all curing ages. The samples made with type I cement exhibited a significantly higher degree of carbonation from 3 d of curing compared to other samples, with a gradual increase until 14 d of curing, after which no notable changes in the degree of carbonation were observed. Following the samples made with type I cement, the samples made with type IV cement exhibited a relatively high degree of carbonation. The carbonation degree of the samples made with type IV cement increased gradually up to 14 d of curing, showing a sharp increase between 14 and 28 d of curing. In contrast, the samples made with type III cement displayed a much lower carbonation degree compared to the other samples. By correlating the results of the carbonation depth measurements with those of the mechanical strength tests, it can be observed that the carbonation-cured samples made with type III cement exhibited the lowest degree of carbonation, yet developed the highest strength among all samples. In contrast, the carbonation-cured samples made with types I and IV cements showed a markedly higher extent of carbonation at 28 d of curing, but their strengths were inferior to those of the carbonation-cured samples made with type III. By recalling the fact that the steam-cured samples made with type III cement also yielded the highest strengths, alite-rich systems favor environments where hydration and pozzolanic reactions predominate, thereby

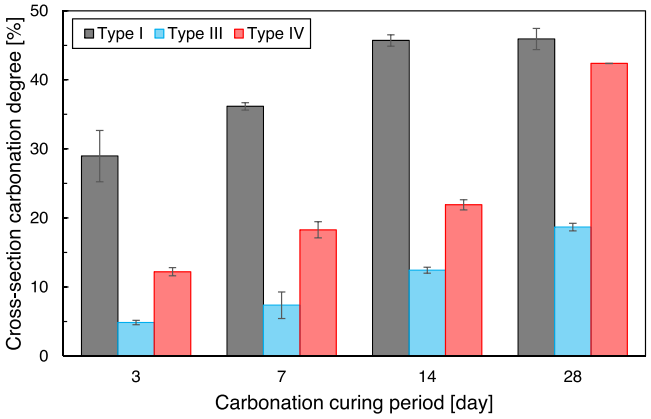

Fig. 9. Cross-section carbonation degree (%) of the carbonation-cured UHPC samples at 28 d of curing.

facilitating the generation of C-S-H. On the other hand, belit-rich systems appeared to benefit more from CO_2 ingress, which promoted the reactivity of clinkers under the carbonation curing. These tendencies were consistently reflected in both compressive and flexural strength development.

3.5. ^{29}Si MAS NMR

The ^{29}Si MAS NMR spectra of the raw materials used in this study are shown in Fig. 10. The raw cement samples exhibited relatively narrow resonance at −71.3 ppm, originating from the unique Si site of belite [65], superimposed on overlapping resonances from alite [66]. The spectrum of type III cement was broadest, while that of type IV cement was sharpest, findings attributable to differences in the relative contents of alite and belite. In the range of approximately −90 – −130 ppm, resonances corresponding to silica fume and silica powder can be observed, both of which belong to the Q^4 band (amorphous SiO_2). Silica powder showed very sharp resonance, whereas silica fume displayed broad resonance over an extended range.

The ^{29}Si MAS NMR spectra of the UHPC paste samples are shown in Fig. 11. The samples at 1 d of curing exhibited characteristic features of C-S-H commonly found in hydrated Portland cement systems [50]. The chain end (Q^1), mid-bridging (Q^2_b), and paired (Q^2_p) sites of the C-S-H chain resonated at −79.4 ppm, −83.5 ppm, and −85.3 ppm, respectively [67,68]. In addition, the mid-group of the C-S-H Si chain, where Si is substituted by Al (Q^2(1Al)), as well as the highly polymerized Si network (Q^3) and the Al-bridged Q^3 (Q^3(1Al)), resonated at −81 ppm, −94 ppm, and −90 ppm, respectively [50]. The samples at 1 d of curing also showed resonance in the Q^0 band, corresponding to the Si in anhydrous clinkers (mainly alite and belite) [65,66], while silica fume and silica powder were still observed in the Q^4 region. Based on the spectral aspects corresponding to C-(A)-S-H, the highest degree of hydration was visually observed in the sample made with type III cement, followed by the samples made with type I and IV cement. This trend can be attributed to the high alite content in type III cement, which promotes rapid hydration.

The ^{29}Si MAS NMR spectra of the steam-cured UHPC samples at 7 d of curing are presented in Fig. 11 (b). Compared to the samples at 1 d of curing, all samples at 7d of curing exhibited a significant increase in the resonance corresponding to C-(A)-S-H. In particular, the Al fractions in the Q^2 and Q^3 sites (Q^2(1Al) and Q^3(1Al)) also showed substantial growth, which is a characteristic feature observed

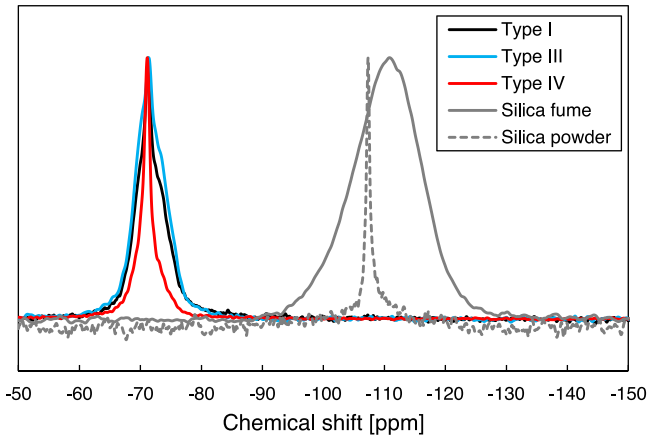

Fig. 10. ^{29}Si MAS NMR spectra of the raw materials used in this study.

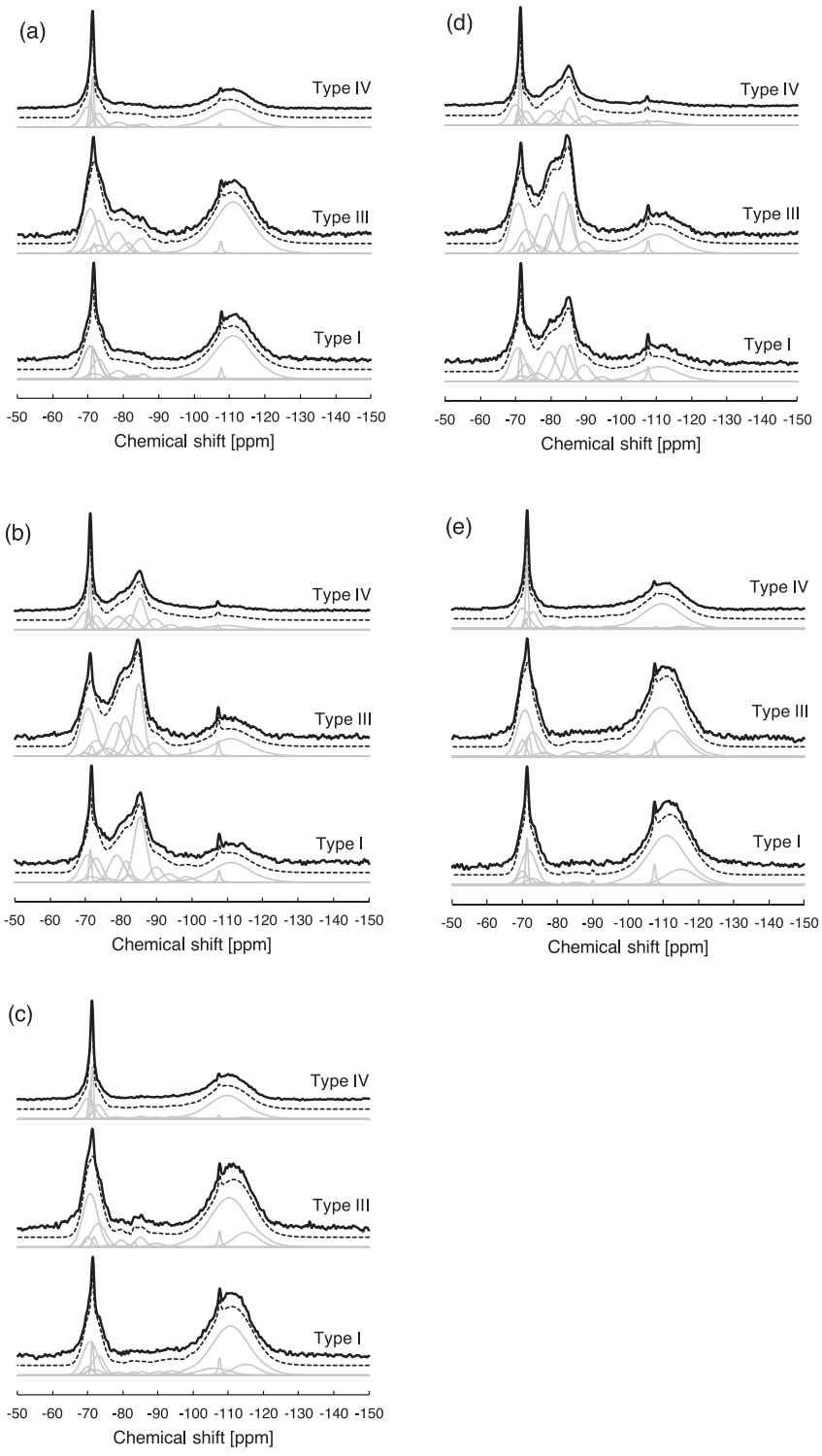

Fig. 11. ^{29}Si MAS NMR spectra of the UHPC paste samples at (a) 1 d of curing, (b) of the steam- and (c) carbonation-cured UHPC paste at 7 d of curing, and (d) of the steam- and (e) carbonation-cured UHPC paste samples at 28 d of curing. Black solid, dotted, and gray lines indicate experimental data, fitted spectra, and deconvoluted spectrum, respectively.

in Portland cement-based materials subjected to high-temperature curing [69]. This phenomenon was observed due possibly to the fact that Al dissolved of Al from Al-bearing phases (e.g., ettringite and monosuflate) under the high-temperature curing might have incorporated into C-S-H. Meanwhile, the intensity of the broad Q^4 site associated with silica fume decreased notably, likely due to the extensive participation of silica fume during the pozzolanic reaction during curing. On the other hand, the ^{29}Si MAS NMR results for the carbonation-cured samples at 7 d of curing displayed a markedly different trend. Most of the resonances corresponding to C-(A)-S-H were significantly reduced, while the Q^4 region accounted for a much larger portion of the spectrum. This phenomenon indicates that a substantial portion of the C-(A)-S-H formed at 1 d of curing underwent decalcification due to carbonation curing, transforming into Ca-modified SiO_2 [59]. Although some residual Q^2 species were observed in the carbonation-cured sample made with type III cement, the majority of the C-(A)-S-H was deemed transformed into Q^3 or Q^4 structures.

The ^{29}Si MAS NMR spectra of the samples at 28 d of curing are presented in Fig. 11 (d) and (e). In the steam-cured samples, the intensity of resonance corresponding to C-(A)-S-H increased further, with a notable rise in the resonance associated with the Q^1 sites. In contrast, the spectra of the carbonation-cured samples showed almost no resonance in the bands corresponding to C-(A)-S-H. Instead, only resonances associated with Si networks exhibiting higher degrees of polymerization, in this case Q^3 and Q^4, were observed.

The deconvolution results (Si fraction (%)) of the ^{29}Si MAS NMR spectra of the UHPC paste samples are summarized in Table 3. In the samples at 1 d of curing, the Si fraction corresponding to the Q^0 sites was lowest in the sample made with type III cement. In contrast, the Si fraction of the Q^0 sites in the samples made with type I and IV cement showed no significant difference. Meanwhile, the Si fraction corresponding to silica fume decreased proportionally to the Si fraction of the Q^0 sites. This suggests that a higher degree of clinker hydration would have resulted in increased portlandite formation, which subsequently participated in the pozzolanic reaction with silica fume to form C-(A)-S-H. Given that the presence of portlandite was not distinctly observed in the XRD and TGA results, it can be inferred that the majority of the portlandite formed was consumed during the pozzolanic reaction.

The ^{29}Si MAS NMR results of the steam-cured samples at 7 d of curing revealed a significant increase in the Si fractions corresponding to Q^2 and Q^3(1Al) compared to the samples at 1 d of curing. This is likely related to the high curing temperature and its influence on silicate chain connectivity [67,69]. Particularly, the fraction of Q^2(1Al) was calculated and found to be higher in the steam-cure samples made with type III cement than in the other samples, indicating greater Al incorporation in C-S-H. It should be noted that the resonance observed at −99 ppm corresponds to silicon from Q^3 or Q^4 sites in silica fume [69]. These resonances are presumed to result from the partial depolymerization (hydrolysis) of Q^4 sites in silica fume due to the high curing temperature [69]. This interpretation is supported by the fact that these resonances were either not detected or found to be negligible in samples at 1 d of curing and in the carbonation-cured samples [69]. In contrast, the carbonation-cured samples exhibited notably lower intensities for the resonances corresponding to C-(A)-S-H. Instead, the Si fraction in the Q^4 region was predominantly occupied by Ca-modified SiO_2, which represents the decalcified form of C-(A)-S-H [59]. Unlike the steam-cured samples, most of the silica fume in the carbonation-cured samples remained unreacted, indicating a lower degree of pozzolanic reaction under the carbonation-curing condition. This clearly suggests that the overall formation of C-S-H was limited, as the curing regime did not provide conditions favorable for pozzolanic reactions (such as those typically promoted under steam curing). Moreover, the majority of the C-S-H that did form was substantially decalcified, which partly accounts for the low strength development observed in the carbonation-cured samples [70–72]. However, given that the Si fractions of Q^0 in the carbonation-cured samples were comparable to those of the steam-cured samples, it can be inferred that the formation of C-(A)-S-H and Ca-modified SiO_2 in the carbonation-cured samples resulted primarily from the direct carbonation of clinkers rather than from the pozzolanic reaction between hydration portlandite and silica fume [73]. Although quantitative XRD results indicated higher reaction degrees of clinkers in the carbonation-cured samples compared to the steam-cured samples, the ^{29}Si MAS NMR deconvolution results did not exhibit a remarkable difference or show a discernible trend.

Table 3
Deconvolution Results (Si fraction (%)) of the ^{29}Si MAS NMR Spectra of the UHPC Paste Samples.

Curing age	Cement type	Curing regime	Si site										
			Q^0	Q^1	Q^2(1Al)	Q^2b	Q^2p	Q^3(1Al)	Q^3	-99	Silica fume	Silica powder	Ca-modified SiO_2
1 d	Type I		34.5	4.2	1.0	1.2	1.6	0.4	0	0	55.6	1.5	0
	Type III		32.4	7.7	2.7	0.2	4.7	0.4	0.1	0	50.6	1.1	0
	Type IV		34.1	4.7	1.2	1.4	2.0	0.3	0.1	0	55.0	1.2	0
7 d	Type I	SC*	25.3	11.1	5.6	7.2	17.4	5.4	3.4	2.0	21.4	1.2	0
		CC**	23.7	1.5	0.7	0.7	1.0	2.4	2.7	0.3	53.3	1.7	12.0
	Type III	SC	24.7	12.2	11.9	7.7	17.8	7.4	0	0	16.9	1.4	0
		CC	27.5	2.1	0.7	1.0	2.6	2.9	1.3	0	49.1	1.5	11.3
	Type IV	SC	27.1	13.2	4.7	10.1	19.0	8.1	3.7	2.5	10.0	1.6	0
		CC	30.7	1.4	0.7	0.8	1.8	2.8	2.2	0.9	55.0	0.8	2.9
28 d	Type I	SC	22.8	13.5	3.0	10.2	21.5	7.0	1.7	0.7	17.9	1.7	0
		CC	22.0	1.5	0.7	0.6	2.0	1.8	0	0	52.3	2.2	16.9
	Type III	SC	26.2	13.1	7.0	20.4	10.4	3.7	1.0	0	17.1	1.1	0
		CC	25.8	1.5	0	0	2.3	1.3	2.8	0.4	45.6	1.4	18.9
	Type IV	SC	28.2	12.2	3.0	12.3	18.3	8.6	3.9	2.4	9.9	1.2	0
		CC	27.5	1.8	0	0.5	2.5	2.0	3.0	0	54.9	0.4	7.4

* Steam curing
** Carbonation curing

Nevertheless, the Si fraction of silica fume in the carbonation-cured sample made with type III cement was lowest, meaning that the higher reaction degree of clinkers before carbonation curing (i.e., 1 d of curing) led to a greater extent of the pozzolanic reaction. Overall, the Si fractions of silica fume in the carbonation-cured samples remained significantly higher than those in the steam-cured samples.

The deconvolution results of the steam-cured samples at 28 d of curing showed little change in terms of the hydration degree compared to the those at 7 d of curing, indicating that the most of the reactions in the steam-cured samples occurred before 7 d of curing. In contrast, the Si fraction corresponding to Q^0 sites in the carbonation-cured samples at 28 d of curing exhibited a further decrease compared to the samples at 7 d of curing. This calculation indicates that carbonation curing continued to induce carbonation of the samples. Additional evidence of this can be found in the increase of the Si fraction associated with Ca-modified SiO_2. Meanwhile, throughout the experimental results, the Si fractions of silica powder showed either consistent or no noticeable trend over the curing period, suggesting that the silica powder did not actively participate in the reaction.

In order to gain a better understanding of the Si network in the samples, calculations of the mean chain length (MCL), the Al/Si of crosslinked C-(A)-S-H, the degree of C-(A)-S-H connectivity (D_c), and the degree of hydration (D_h) were calculated and are tabulated in Table 4. Overall, the MCL values of the carbonation-cured samples were higher than those of the steam-cured samples. This can be attributed to the formation of C-(A)-S-H with a lower Ca/Si ratio, which was promoted during the decalcification process of C-(A)-S-H during carbonation [74]. Consequently, the increase in Al/Si led to a subsequent rise in the MCL values [75]. The MCL values of the carbonation-cured samples were highest in those made with type IV cement, indicating that CO_2 was more effectively facilitated in the samples made with type IV cement, thus having a more notable impact on the hydration products. Meanwhile, the D_c value is an index used to assess the polymerization degree of C-S-H and is influenced by Ca/Si and the interlayered water of C-S-H [76–78]. The D_c value increased significantly in the carbonation-cured samples, mainly due to the reduced Ca/Si in C-S-H [76–78]. The D_h values were calculated and found to be considerably higher in the steam-cured samples than in the carbonation-cured samples. While the D_h value increased gradually in the carbonation-cured samples up to 28 d, it should be noted that the D_h values of the carbonation-cured samples were based on the Si fractions of the hydration products and Ca-modified SiO_2. Therefore, one should interpret D_h with caution, and this variable should be used for reference only.

3.6. Perspectives

This study investigated the potential for the application of carbonation curing to produce UHPC made with three different types of Portland cement. Based on experimental results, it was estimated that steam curing not only promotes the hydration of cement but also facilitates the pozzolanic reaction with silica fume, making the use of type III cement most advantageous in terms of the mechanical properties and degree of the reaction. When carbonation curing was used as an alternative to steam curing in producing UHPC, however, the mechanical strength of the samples was lower than the corresponding outcomes for the steam-cured samples. Nevertheless, environmental benefits, such as CO_2 uptake, must be taken into consideration when applying carbonation curing to UHPC. Carbonation-cured samples made with type I and IV cements proved to be effective in terms of CO_2 uptake. In addition, based on the quantitative XRD analysis, carbonation curing remarkably improved the reaction degrees of clinkers in the samples made with type IV cement. This observation aligns fairly well with earlier works that demonstrated that the reaction degree of belite is significantly enhanced upon carbonation curing [44,80–82]. Furthermore, considering the fact that the calcination temperature of belite is lower

Table 4
Mean Chain Length, Al/Si of Crosslinked C-(A)-S-H, Degree of C-(A)-S-H Connectivity, and Degree of Hydration (%) of the UHPC paste samples as calculated from the ^{29}Si MAS NMR deconvolution results.

Curing age	Cement type	Curing regime	MCL*	Al/Si**	Dc***	Dh**** (%)
1 d	Type I		8.25	0.04	1.40	8.23
	Type III		8.48	0.03	1.41	15.85
	Type IV		8.49	0.03	1.44	9.69
7 d	Type I	SC*****	20.02	0.11	1.80	50.00
		CC******	29.80	0.27	2.20	20.99
	Type III	SC	21.05	0.13	1.68	56.94
		CC	25.56	0.27	1.89	21.84
	Type IV	SC	20.27	0.14	1.79	58.88
		CC	35.01	0.29	2.13	12.54
28 d	Type I	SC	18.96	0.12	1.75	56.75
		CC	22.45	0.28	1.63	23.49
	Type III	SC	18.15	0.07	1.73	55.61
		CC	24.64	0.17	2.20	26.80
	Type IV	SC	21.97	0.15	1.82	58.37
		CC	26.21	0.20	2.15	17.14

* Mean chain length = $4(Q^1 + Q^2 + Q^2(1Al) + Q^3 + 2Q^3(1Al))/Q^1$ [75]
** Al/Si of crosslinked C-(A)-S-H = $Q^3(1Al)/(Q^1 + Q^2 + Q^2(1Al) + Q^3 + Q^3(1Al))$ [75]
*** Degree of C-(A)-S-H connectivity = $(Q^1 + 2Q^2 + 3Q^3)/(Q^1 + Q^2 + Q^3)$ [79]
**** Degree of hydration = $Q^1 + Q^2(1Al) + Q^2 + Q^3(1Al) + Q^3$ + Ca-modified SiO_2 [79]
***** Steam curing
****** Carbonation curing

than that of alite, the samples made with belite-rich cement are deemed environmentally friendly. Therefore, applying carbonation curing to UHPC made with type IV cement is almost certainly the most efficient approach. In contrast, the carbonation-cured samples made with type III cement in this study exhibited the lowest degree of CO_2 ingress relative to the other samples. This can be attributed to the high reactivity of clinkers of type III cement prior to carbonation curing, which limits the potential for CO_2 penetration.

Meanwhile, as observed in the ^{29}Si MAS NMR results, the role of silica fume in the carbonation-cured samples is highly limited, as it exhibits very low pozzolanic reactivity. Consequently, silica fume may behave more like an inert filler, similar to silica powder. Nevertheless, the pozzolanic reaction was evidently suppressed under the carbonation curing, resulting in the formation of only a limited amount of C-S-H. As C-S-H generally serves as the main strength-giving phase in typical UHPC, its deficiency clearly accounted for the reduced mechanical performance of carbonation-cured samples. Furthermore, the formed C-S-H underwent extensive decalcification during the carbonation curing, thereby precluding the possibility of achieving strength levels comparable to those of steam-cured counterparts within the mixture design adopted in this study. Therefore, when applying carbonation curing to produce UHPC, adjustments of the quantities of supplementary materials, such as silica fume and silica powder, as well as the cement content, should be made according to the specific applications so as to optimize the properties of UHPC.

Beyond the mechanical performances, carbonation curing offers significant environmental advantages over conventional steam curing. The quantification of CO_2 uptake in the carbonation-cured UHPC samples made with type I, III, and IV cements reached 7.1 %, 4.6 %, and 7.7 %, respectively, relative to binder mass, corresponding to approximately 46 – 77 kg CO_2/m^3 permanently mineralized in the hardened carbonation-cured UHPC matrix [83]. This sequestration has the potential to offset a considerable fraction of the embodied carbon of the PC clinkers (0.8 – 0.9 ton CO_2 per ton of PC) and directly contributes to reducing the net greenhouse gas footprint of UHPC production [84]. To rigorously quantify these environmental trade-offs, future work should incorporate a cradle-to-gate life cycle assessment that can balance: 1) the avoided energy demand of steam curing; 2) the permanent CO_2 uptake; and 3) the mechanical performance implications. Recent studies have demonstrated that such integrated assessments are critical to positioning carbonation curing as a viable and sustainable alternative for concrete production in industrial practice [85,86].

4. Conclusion

The effect of Portland cement type on the properties of carbonation-cured UHPC was explored in this study. UHPC samples underwent steam curing for 2 d or carbonation curing for 27 d. The applicability of carbonation curing during the fabrication of UHPC was evaluated by means of compressive and flexural strength measurements, XRD, TGA, carbonation depth, and ^{29}Si MAS NMR tests. Based on the experimental results, the following conclusions were drawn:

(1) The mechanical strength of the carbonation-cured UHPC samples was generally lower compared to that of the steam-cured UHPC samples.
(2) The CO_2 ingress and uptake of the UHPC samples made with type I and IV cement were higher than those of the UHPC samples made with type III cement.
(3) Continuous carbonation curing gradually promoted reactivity in the carbonation-cured UHPC samples.
(4) The formation of a substantial quantity of C-(A)-S-H was found in the steam-cured UHPC samples made with type III and IV cement, resulting in higher mechanical strength.
(5) Given that silica fume contributed very little to the reactions in the carbonation-cured UHPC samples, strength development was primarily driven by the carbonation of clinkers, which led to the formation of C-S-H and the precipitation of $CaCO_3$.

These results suggest that the carbonation curing of UHPC, particularly with belite-rich cement, could provide a low-energy and low-carbon alternative to conventional steam curing practices, thereby offering practical value for sustainable construction applications. However, future research should focus on the optimization of certain curing conditions, such as the CO_2 concentration, and on the limited role of silica fume during carbonation curing, as well as the development of integrated assessments to positioning carbonation curing as a viable and sustainable alternative for UHPC production in industrial practice.

CRediT authorship contribution statement

H.K. Lee: Writing – review & editing, Supervision, Project administration, Investigation, Funding acquisition, Formal analysis, Data curation, Conceptualization. **Naru Kim:** Writing – original draft, Visualization, Investigation. **Sungsik Choi:** Writing – review & editing, Formal analysis, Data curation. **Jihoon Park:** Writing – original draft, Visualization, Data curation, Conceptualization. **Jin-Ho Bae:** Writing – original draft, Investigation, Formal analysis, Data curation. **Joonho Seo:** Writing – review & editing, Writing – original draft, Methodology, Investigation, Formal analysis, Data curation, Conceptualization. **G.M. Kim:** Writing – original draft, Methodology, Investigation, Formal analysis, Conceptualization.

Declaration of Competing Interest

The authors declare that they have no known competing financial interests or personal relationships that could have appeared to influence the work reported in this paper.

Acknowledgments

This research was supported by the National Research Foundation (NRF) of the Korean government (Ministry of Science & ICT) [No. RS-2026-25481306].

Data availability

The data that has been used is confidential.

References

[1] J. Tamošaitienė, S. Parham, H. Sarvari, D.W. Chan, D.J. Edwards, A review of the application of synthetic and natural polymers as construction and building materials for achieving sustainable construction, Buildings 14 (8) (2024) 2569.
[2] J. Du, W. Meng, K.H. Khayat, Y. Bao, P. Guo, Z. Lyu, A. Abu-Obeidah, H. Nassif, H. Wang, New development of ultra-high-performance concrete (UHPC), Compos. Part B Eng. 224 (2021) 109220.
[3] R. Ullah, Y. Qiang, J. Ahmad, N.I. Vatin, M.A. El-Shorbagy, Ultra-high-performance concrete (UHPC): A state-of-the-art review, Materials 15 (12) (2022) 4131.
[4] I.-H. Yang, J. Park, Mechanical and thermal properties of UHPC exposed to high-temperature thermal cycling, Adv. Mater. Sci. Eng. 2019 (1) (2019) 9723693.
[5] J. Li, Z. Wu, C. Shi, Q. Yuan, Z. Zhang, Durability of ultra-high performance concrete–A review, Constr. Build. Mater. 255 (2020) 119296.
[6] F. Dingqiang, Y. Rui, S. Zhonghe, W. Chunfeng, W. Jinnan, S. Qiqi, A novel approach for developing a green Ultra-High Performance Concrete (UHPC) with advanced particles packing meso-structure, Constr. Build. Mater. 265 (2020) 120339.
[7] R. Yu, P. Spiesz, H. Brouwers, Effect of nano-silica on the hydration and microstructure development of Ultra-High Performance Concrete (UHPC) with a low binder amount, Constr. Build. Mater. 65 (2014) 140–150.
[8] S. Park, S. Wu, Z. Liu, S. Pyo, The role of supplementary cementitious materials (SCMs) in ultra high performance concrete (UHPC): A review, Materials 14 (6) (2021) 1472.
[9] Y. Dong, Performance assessment and design of ultra-high performance concrete (UHPC) structures incorporating life-cycle cost and environmental impacts, Constr. Build. Mater. 167 (2018) 414–425.
[10] J. Li, X. Wang, D. Chen, D. Wu, Z. Han, D. Hou, Z. Zhen, C. Peng, Q. Ding, B. Yin, Design and application of UHPC with high abrasion resistance, Constr. Build. Mater. 309 (2021) 125141.
[11] M. Amran, S.-S. Huang, A.M. Onaizi, N. Makul, H.S. Abdelgader, T. Ozbakkaloglu, Recent trends in ultra-high performance concrete (UHPC): Current status, challenges, and future prospects, Constr. Build. Mater. 352 (2022) 129029.
[12] I. Won, Y. Na, J.T. Kim, S. Kim, Energy-efficient algorithms of the steam curing for the in situ production of precast concrete members, Energy Build. 64 (2013) 275–284.
[13] S. Türkel, V. Alabas, The effect of excessive steam curing on Portland composite cement concrete, Cem. Concr. Res. 35 (2) (2005) 405–411.
[14] C. Tashiro, H. Tanaka, The effect of the lowering of initial curing temperature on the strength of steam cured mortar, Cem. Concr. Res. 7 (5) (1977) 545–551.
[15] T. Chen, X. Gao, Effect of carbonation curing regime on strength and microstructure of Portland cement paste, J. CO2 Util. 34 (2019) 74–86.
[16] J. Wang, H. Xu, D. Xu, P. Du, Z. Zhou, L. Yuan, X. Cheng, Accelerated carbonation of hardened cement pastes: Influence of porosity, Constr. Build. Mater. 225 (2019) 159–169.
[17] S. Siddique, A. Naqi, J.G. Jang, Influence of water to cement ratio on CO2 uptake capacity of belite-rich cement upon exposure to carbonation curing, Cem. Concr. Compos. 111 (2020) 103616.
[18] C. Moro, V. Francioso, M. Velay-Lizancos, Impact of nano-TiO2 addition on the reduction of net CO2 emissions of cement pastes after CO2 curing, Cem. Concr. Compos. 123 (2021) 104160.
[19] Y. Meng, T.-C. Ling, K.H. Mo, W. Tian, Enhancement of high temperature performance of cement blocks via CO2 curing, Sci. Total Environ. 671 (2019) 827–837.
[20] Y. Liu, Y. Zhuge, C.W. Chow, A. Keegan, P.N. Pham, D. Li, G. Qian, L. Wang, Recycling drinking water treatment sludge into eco-concrete blocks with CO2 curing: Durability and leachability, Sci. Total Environ. 746 (2020) 141182.
[21] O. Ahmed, S. Ahmad, S.K. Adekunle, Carbon dioxide sequestration in cementitious materials: A review of techniques, material performance, and environmental impact, J. CO2 Util. 83 (2024) 102812.
[22] H. Huang, T. Wang, B. Kolosz, J. Andresen, S. Garcia, M. Fang, M.M. Maroto-Valer, Life-cycle assessment of emerging CO2 mineral carbonation-cured concrete blocks: Comparative analysis of CO2 reduction potential and optimization of environmental impacts, J. Clean. Prod. 241 (2019) 118359.
[23] H. Hamada, A. Alattar, B. Tayeh, F. Yahaya, I. Almeshal, Influence of different curing methods on the compressive strength of ultra-high-performance concrete: A comprehensive review, Case Stud. Constr. Mater. 17 (2022) e01390.
[24] W. Tian, Y. Liu, W. Wang, Multi-structural evolution of conductive reactive powder concrete manufactured by enhanced ohmic heating curing, Cem. Concr. Compos. 123 (2021) 104199.
[25] H. Yazıcı, E. Deniz, B. Baradan, The effect of autoclave pressure, temperature and duration time on mechanical properties of reactive powder concrete, Constr. Build. Mater. 42 (2013) 53–63.
[26] W. Meng, K. Khayat, Effects of saturated lightweight sand content on key characteristics of ultra-high-performance concrete, Cem. Concr. Res. 101 (2017) 46–54.
[27] H. Huang, L. Teng, X. Gao, K.H. Khayat, F. Wang, Z. Liu, Use of saturated lightweight sand to improve the mechanical and microstructural properties of UHPC with fiber alignment, Cem. Concr. Compos. 129 (2022) 104513.
[28] M. Nodehi, S.E. Nodehi, Ultra high performance concrete (UHPC): Reactive powder concrete, slurry infiltrated fiber concrete and superabsorbent polymer concrete, Innov. Infrastruct. Solut. 7 (1) (2022) 39.
[29] J. Justs, M. Wyrzykowski, D. Bajare, P. Lura, Internal curing by superabsorbent polymers in ultra-high performance concrete, Cem. Concr. Res. 76 (2015) 82–90.
[30] D. Shi, Y. Xia, Y. Zhao, X. Ma, J. Wang, M. Liu, K. Yu, Evaluation of technical and gamma radiation shielding properties of sustainable ultra-high performance geopolymer concrete, Constr. Build. Mater. 436 (2024) 137003.
[31] Y. Xia, D. Shi, Y. Zhao, J. Wang, X. Ma, K. Yu, H. Li, L. Wang, J. Yan, Designing low-carbon ultra-high performance concrete with co-combustion ash of sewage sludge and rice husk, Mater. Struct. 58 (1) (2025) 7.
[32] J. Wang, D. Shi, K. Yu, J. Miao, J. Zhang, Y. Zhao, Y. Xia, Efficient recycling of high-volume Waste-to-Energy bottom ash for integration into ultra-high-performance geopolymer concrete, Constr. Build. Mater. 486 (2025) 142020.
[33] L. Hu, Y. Yao, J. Sun, W. Li, Z. Leng, H. Yang, S. Li, Uncovering the role of steel slag in CO2-cured UHPC: Evaluation on impact resistance, carbonation kinetics and microstructure with X-ray CT, Constr. Build. Mater. 472 (2025) 140989.
[34] K.O. Mohaisen, S. Ahmad, S.K. Adekunle, M. Maslehuddin, S.U. Al-Dulaijan, Effect of Curing Methods on the Performance of UHPC, Arab. J. Sci. Eng. 48 (10) (2023) 13791–13805.
[35] M.-Y. Xuan, S.-h Lee, H.-q Hu, X.-Y. Wang, Adding dry ice into ultra-high-performance concrete to enhance engineering performances and lower CO2 emissions, Constr. Build. Mater. 392 (2023) 131858.
[36] A. Hasanbeigi, L. Price, E. Lin, Emerging energy-efficiency and CO2 emission-reduction technologies for cement and concrete production: A technical review, Renew. Sustain. Energy Rev. 16 (8) (2012) 6220–6238.
[37] A. Neville, Maintenance and durability of structures, Concr. Int. 19 (11) (1997) 52–56.

[38] P.K. Mehta, R.W. Burrows, Building durable structures in the 21st century, Concr. Int. 23 (3) (2001) 57–63.
[39] H.A. Dehwah, Influence of cement composition on concrete durability in chloride–sulfate environments, Loughborough University, 1999.
[40] S.A. Altoubat, D.A. Lange, Creep, shrinkage, and cracking of restrained concrete at early age, Acids Mater. J. Am. Concr. Inst. 98 (4) (2001) 323–331.
[41] A.J. Cuberos, G. Ángeles, M.C. Martín-Sedeño, L. Moreno-Real, M. Merlini, L.M. Ordónez, M.A. Aranda, Phase development in conventional and active belite cement pastes by Rietveld analysis and chemical constraints, Cem. Concr. Res. 39 (10) (2009) 833–842.
[42] C. Popescu, M. Muntean, J. Sharp, Industrial trial production of low energy belite cement, Cem. Concr. Compos. 25 (7) (2003) 689–693.
[43] T. Staněk, P. Sulovský, Active low-energy belite cement, Cem. Concr. Res. 68 (2015) 203–210.
[44] J.G. Jang, H.-K. Lee, Microstructural densification and CO2 uptake promoted by the carbonation curing of belite-rich Portland cement, Cem. Concr. Res. 82 (2016) 50–57.
[45] Q. Guan, Y. Ma, M. Jin, H. Zeng, C. Gao, J. Tang, J. Liu, F. Han, W. Li, J. Liu, Carbonation curing of belite-rich cement: the role of fly ash and strengthening mechanism, Cem. Concr. Compos. 149 (2024) 105530.
[46] H. Kim, J. Pei, S. Siddique, J.-G. Jang, Effects of the curing conditions on the carbonation curing efficiency of ordinary Portland cement and a belite-rich cement mortar, Sustainability 13 (9) (2021) 5175.
[47] C.J. Goodbrake, J.F. Young, R.L. Berger, Reaction of beta-dicalcium silicate and tricalcium silicate with carbon dioxide and water vapor, J. Am. Ceram. Soc. 62 (3-4) (1979) 168–171.
[48] J. Ibanez, L. Artús, R. Cuscó, Á. López, E. Menéndez, M.C. Andrade, Hydration and carbonation of monoclinic C2S and C3S studied by Raman spectroscopy, J. Raman Spectrosc. Int. J. Orig. Work all Asp. Raman Spectrosc. Incl. High. Order Process. also Brillouin Rayleigh Scatt. 38 (1) (2007) 61–67.
[49] A. ASTM, C150/C150M-17, standard specification for Portland cement, Am. Soc. Test. Mater. West Conshohocken, PA, USA (2017).
[50] N.K. Lee, K. Koh, M.O. Kim, G. Ryu, Uncovering the role of micro silica in hydration of ultra-high performance concrete (UHPC), Cem. Concr. Res. 104 (2018) 68–79.
[51] J.W. Bullard, H.M. Jennings, R.A. Livingston, A. Nonat, G.W. Scherer, J.S. Schweitzer, K.L. Scrivener, J.J. Thomas, Mechanisms of cement hydration, Cem. Concr. Res. 41 (12) (2011) 1208–1223.
[52] A. ASTM, C109/C109M-Standard Test Method for Compressive Strength of Hydraulic Cement Mortars (Using 2-in. Or (50-mm) Cube Specimens); 2013. 2, Scope of Work Shall Include but not be Limited to the Following:-Suspende d Metal Grid for Acoustical Tile Ceiling System (1999).
[53] A. C348, Standard test method for flexural strength of hydraulic-cement mortars, American Society for Testing and Materials International, West Conshohocken, Pennsylvania, United States (2008).
[54] A. Standard, Standard practice for fabricating and testing specimens of ultra-high performance concrete, ASTM International, West Conshohocken, PA (2017).
[55] F.A. Hartmann, J. Plank, New insights into the effects of aging on Portland cement hydration and on retarder performance, Constr. Build. Mater. 274 (2021) 122104.
[56] T. Oertel, U. Helbig, F. Hutter, H. Kletti, G. Sextl, Influence of amorphous silica on the hydration in ultra-high performance concrete, Cem. Concr. Res. 58 (2014) 121–130.
[57] Z. Chen, T. Zhang, Y. WU, I. Madsen, J. Ma, K. Sagoe-Crentsil, A. Neild, W. Duan, In-Situ Xrd Study of the Effects of Amino Acids on the Carbonation Kinetics of Cementitious Calcium Silicates, Available at SSRN 5069197.
[58] H.F. Taylor, Cement chemistry, Thomas Telford London1997.
[59] J. Seo, S.M. Park, H.-K. Lee, Evolution of the binder gel in carbonation-cured Portland cement in an acidic medium, Cem. Concr. Res. 109 (2018) 81–89.
[60] D. Silva, H. Roman, P. Gleize, Evidences of chemical interaction between EVA and hydrating Portland cement, Cem. Concr. Res. 32 (9) (2002) 1383–1390.
[61] J. Dweck, P.M. Buchler, A.C.V. Coelho, F.K. Cartledge, Hydration of a Portland cement blended with calcium carbonate, Thermochim. Acta 346 (1-2) (2000) 105–113.
[62] B. Lu, S. Drissi, J. Liu, X. Hu, B. Song, C. Shi, Effect of temperature on CO2 curing, compressive strength and microstructure of cement paste, Cem. Concr. Res. 157 (2022) 106827.
[63] I. Galan, C. Andrade, M. Castellote, Thermogravimetrical analysis for monitoring carbonation of cementitious materials: Uptake of CO 2 and deepening in C–S–H knowledge, J. Therm. Anal. Calorim. 110 (1) (2012) 309–319.
[64] J. Branch, D. Kosson, A. Garrabrants, P. He, The impact of carbonation on the microstructure and solubility of major constituents in microconcrete materials with varying alkalinities due to fly ash replacement of ordinary Portland cement, Cem. Concr. Res. 89 (2016) 297–309.
[65] K. Jost, B. Ziemer, R. Seydel, Redetermination of the structure of β-dicalcium silicate, Struct. Sci. 33 (6) (1977) 1696–1700.
[66] S.L. Poulsen, V. Kocaba, G. Le Saoût, H.J. Jakobsen, K.L. Scrivener, J. Skibsted, Improved quantification of alite and belite in anhydrous Portland cements by 29Si MAS NMR: effects of paramagnetic ions, Solid State Nucl. Magn. Reson. 36 (1) (2009) 32–44.
[67] R.J. Myers, E. L'Hôpital, J.L. Provis, B. Lothenbach, Effect of temperature and aluminium on calcium (alumino) silicate hydrate chemistry under equilibrium conditions, Cem. Concr. Res. 68 (2015) 83–93.
[68] J. Skibsted, M.D. Andersen, The effect of alkali ions on the incorporation of aluminum in the calcium silicate hydrate (C–S–H) phase resulting from Portland cement hydration studied by 29 Si MAS NMR, J. Am. Ceram. Soc. 96 (2) (2013) 651–656.
[69] T. Bach, C.C.D. Coumes, I. Pochard, C. Mercier, B. Revel, A. Nonat, Influence of temperature on the hydration products of low pH cements, Cem. Concr. Res. 42 (6) (2012) 805–817.
[70] N. Li, N. Farzadnia, C. Shi, Microstructural changes in alkali-activated slag mortars induced by accelerated carbonation, Cem. Concr. Res. 100 (2017) 214–226.
[71] L. Li, Q. Liu, V. Dao, M. Wu, Dimensional change of cement paste subjected to carbonation in CO2 sequestration and utilization context: A critical review on the mechanisms, J. CO2 Util. 70 (2023) 102444.
[72] T.N. Nguyen, Q.T. Phung, L. Frederickx, D. Jacques, A. Dauzeres, J. Elsen, Y. Pontikes, Microstructural evolution and its impact on the mechanical strength of typical alkali-activated slag subjected to accelerated carbonation, Dev. Built Environ. 19 (2024) 100519.
[73] J.K. Weng, B. Langan, M. Ward, Pozzolanic reaction in Portland cement, silica fume, and fly ash mixtures, Can. J. Civ. Eng. 24 (5) (1997) 754–760.
[74] B. Lothenbach, K. Scrivener, R. Hooton, Supplementary cementitious materials, Cem. Concr. Res. 41 (12) (2011) 1244–1256.
[75] R.J. Myers, S.A. Bernal, R. San Nicolas, J.L. Provis, Generalized structural description of calcium–sodium aluminosilicate hydrate gels: the cross-linked substituted tobermorite model, Langmuir 29 (17) (2013) 5294–5306.
[76] X. Cong, R.J. Kirkpatrick, 29Si MAS NMR study of the structure of calcium silicate hydrate, Adv. Cem. Based Mater. 3 (3-4) (1996) 144–156.
[77] G. Bell, J. Bensted, F. Glasser, E. Lachowski, D. Roberts, M. Taylor, Study of calcium silicate hydrates by solid state high resolution 29Si nuclear magnetic resonance, Adv. Cem. Res. 3 (9) (1990) 23–27.
[78] A. Korpa, S. Dervishi, J. Volavsek, S. Gjyli, A. Andoni, 29Si and 27Al MAS NMR assessment of the C-(A-) S–H nanomolecular structure of Ultra-High-Performance Concrete (UHPC) modified with pyrogenic oxides, J. Indian Chem. Soc. 99 (6) (2022) 100443.
[79] J.J. Kim, M.K. Rahman, A.A. Al-Majed, M.M. Al-Zahrani, M.M.R. Taha, Nanosilica effects on composition and silicate polymerization in hardened cement paste cured under high temperature and pressure, Cem. Concr. Compos. 43 (2013) 78–85.
[80] K.K. Das, J. Pei, R. Sharma, X. Wu, J.G. Jang, Influence of silica fume and lime on belite-rich cement paste subjected to atmospheric and autoclave CO2 curing regime, Constr. Build. Mater. 436 (2024) 136909.
[81] J. Seo, S. Kim, S. Park, H.N. Yoon, H.-K. Lee, Carbonation of calcium sulfoaluminate cement blended with blast furnace slag, Cem. Concr. Compos. 118 (2021) 103918.
[82] J. Seo, S. Kim, D. Jang, H. Kim, H. Lee, Internal carbonation of belite-rich Portland cement: An in-depth observation at the interaction of the belite phase with sodium bicarbonate, J. Build. Eng. 44 (2021) 102907.
[83] M. Zhou, Z. Wu, X. Ouyang, X. Hu, C. Shi, Mixture design methods for ultra-high-performance concrete-a review, Cem. Concr. Compos. 124 (2021) 104242.

[84] S.A. Miller, V.M. John, S.A. Pacca, A. Horvath, Carbon dioxide reduction potential in the global cement industry by 2050, Cem. Concr. Res. 114 (2018) 115–124.
[85] D. Shi, J. Miao, Y. Xia, J. Wang, F. Chen, X. Ma, K. Yu, C. Sun, W. Tian, Valorization of sewage sludge ash into sustainable porous geopolymer: Dual functions as supplementary foaming agent and precursor, Environ. Res. (2025) 122431.
[86] D. Kamath, X. Zhao, K.O. Armstrong, P.B. Anleu, H. Sun, R.U. Martinez, M.P. Paranthaman, Towards low-carbon low-energy concrete alternatives: Life cycle assessment of carbonated cementitious material-based precast panels, Sci. Total Environ. 976 (2025) 179279.